ELSEVIER

Surface Science 443 (1999) 133–153

surface science

www.elsevier.nl/locate/susc

Theoretical study of the termination of the Fe_3O_4 (111) surface

Jamila Ahdjoudj [a], Cyril Martinsky [a], Christian Minot [a,*], Michel A. Van Hove [b,c], Gabor A. Somorjai [b,d]

[a] *Laboratoire de Chimie Théorique, UMR 7616 CNRS, Tour 23-22, Boîte 137, Université P. et M. Curie, 75252 Paris, Cédex 05, France*
[b] *Materials Sciences Division, Lawrence Berkeley National Laboratory, University of California, Berkeley, CA 94720, USA*
[c] *Department of Physics, University of California, Davis, CA 95616, USA*
[d] *Department of Chemistry, University of California, Berkeley, CA 94720, USA*

Received 23 April 1999; accepted for publication 14 September 1999

Abstract

Ab-initio periodic Hartree–Fock calculations for the structure of the (111) surface of Fe_3O_4 (magnetite) are presented. The slabs that are derived by an ideal bulk truncation that leaves one or two iron monolayers outside oxygen layers are found to be more stable than others since they preserve most of the coordination of the surface atoms. The stability of the slabs that represent the surface layers depends on the overall composition, specifically on the deviation from stoichiometry, and on the dipole moment perpendicular to the surface. The symmetrical slab with the layer sequence $Fe_2O_4Fe_3O_4Fe_2$, terminated on each side by iron bilayers, is the best compromise since symmetry insures the neutrality of the dipole moment. This slab is oxygen-deficient. The energetically preferred structure relaxes so that one of the two outermost iron layers moves toward the slab center plane, exchanging sequence with the oxygen layer. The slab with the layer sequence $FeO_4Fe_3O_4Fe$, which is also symmetric, is terminated by iron single monolayers, would represent an excessive oxidation of the iron atoms. This slab may be reduced by hydrogenation; it is then strongly stabilized and the vertical displacement of the oxygen atoms agrees with the structure determined by LEED (the LEED study would not have detected hydrogen).

Keywords: CRYSTAL; Iron oxide; Polar surface; Relaxation; UHF

1. Introduction

Magnetite, Fe_3O_4, is one of the most important and most abundant transition metal oxides. It plays a major role in corrosion and is extensively used for magnetic storage of information [1]. The surface properties of iron oxides are used in corrosion control [2] and heterogeneous catalysis [3]. The knowledge of the structure of a few monolayers of Fe_3O_4 grown from an iron vapor in an oxygen atmosphere is useful to predict the reactivity of adsorbates on Fe_3O_4.

An understanding of the atomic scale structure and energetics of oxide surfaces is the first step to explain processes like adsorption, catalysis and corrosion. Many metal oxides do not reconstruct, i.e. their surfaces essentially retain the bulk structure. This is not the case for polar surfaces classified as type 3 that have a dipole moment perpendicular to the surface [4]. These surfaces can be seen as a stack of layers that contain either only pure metal cations or pure oxygen anions. While non-polar surfaces have an an amphoteric

* Corresponding author. Fax: +33-1-44274117.
E-mail address: minot@lct.jussieu.fr (C. Minot)

0039-6028/99/$ - see front matter
PII: S0039-6028(99)01008-0

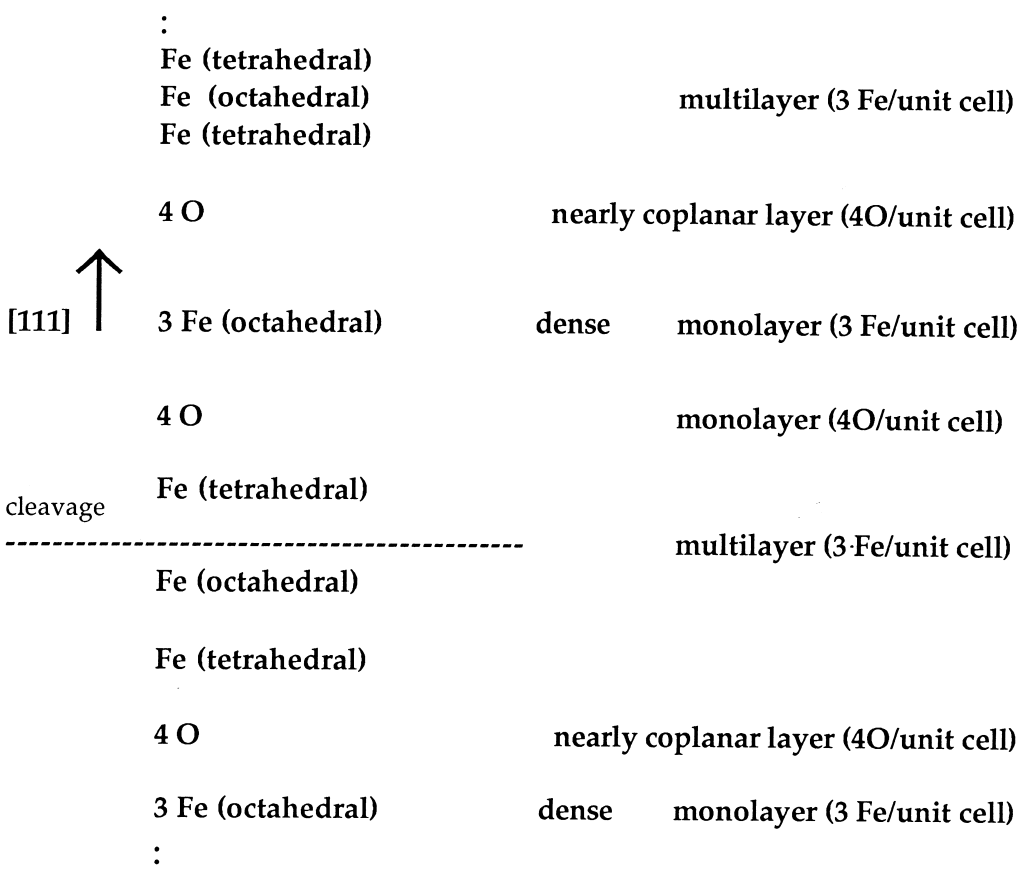

Fig. 1. Stacking of Fe_3O_4 along the [111] orientation with atomic density expressed as atoms per two-dimensional unit cell. Monolayers and multilayers are defined as near-coplanar and non-coplanar layers. Iron atoms are bonded either tetrahedrally or octahedrally to four or six O atoms, respectively, as indicated. The energetically most favourable cleavage cuts through an iron multilayer and is indicated by a dashed line and generates two surfaces terminated by one or two iron monolayer.

character, these surfaces have only anionic or cationic sites. The structure determination of the surface layer allows one to know the accessible active site for catalysis. The stacking of layers with opposite charges could be seen as capacitors linked in series, developing macroscopic charges and giving rise to a large dipole moment. A drastic relaxation makes it possible to decrease the dipole moment perpendicular to the surface. The Fe_3O_4 (111) surface is of type 3, as described in Fig. 1 (see Section 4 for details), and one problem in calculating the most stable termination of this oxide with this orientation results from the instability due to the dipole moment normal to the surface. In addition, the iron cations are in high spin states that require unrestricted Hartree–Fock wave functions (UHF) unavailable recently with periodic HF methods. Using the last release of the CRYSTAL program [5], it is now possible to calculate the wave functions.

Surfaces of other iron oxides have been prepared by cleavage or by epitaxial growth and have been characterized [6–8]. The oxygen pressure plays a role in the conversion of one oxide into another. A single bilayer of FeO was deposited on different faces of platinum. On Pt(111), a 15% mismatch between the hexagonal lattice parameters imposed a superstructure. This FeO bilayer is found experimentally to be terminated by an oxygen monolayer [9–11]. A preliminary theoreti-

cal study, not reported here in detail, shows that the stoichiometric slabs with the bulk parameters terminated by ordered half monolayers of oxygen (a 2×1 ordering with every other oxygen atom missing) are more stable than those terminated by half monolayers of iron. These surfaces are shown to adsorb water and lead very easily to termination by full monolayers of OH groups. The top surface of α-$Cr_2O_3(0001)$, Cr^{3+}-terminated, undergoes a dramatic relaxation of the top layer that moves inward by 50% of the original spacing [12]. Experimentally, the α-Fe_2O_3 $(\bar{1}012)$ face relaxes and is deficient in oxygen [13]. The relaxation extends to 30 Å in depth. The α-Fe_2O_3 (0001) face is stable, is found in naturally grown hematites, and has been studied by Weiss et al. [14–16]. After treatment (see below), it is covered by a Fe_3O_4 (111) layer [17,18]. Some theoretical studies for (0001) α-Fe_2O_3 have been perfomed using potentials [19], cluster approaches [20] and, recently, spin density functional theory [21]. CRYSTAL slab models for (0001) and $(10\bar{1}0)$ α-Fe_2O_3 hematite [22] or other hematite crystals (α-Cr_2O_3 [12,23] or α-Al_2O_3 [24]) have been discussed.

The predominant natural growth faces of Fe_3O_4 are (111) and (100). Experimentally, the structure of the (111) surface of Fe_3O_4 has been studied by dynamical LEED [18,25], by STM[26,27] and by photoelectron diffraction (PD) [9]. For the first study, the surface is prepared epitaxially layer by layer: after deposition of each monolayer of iron onto a Pt(111) surface, it is oxidized and heated to generate an ordered oxide layer [6,25]. After several layer-by-layer depositions, a bulk-like oxide is formed with composition Fe_3O_4, whose thickness is controlled. In the PD study [9], the same procedure was followed, except that the deposition was not done layer by layer: a multilayer Fe film was oxidized all at once. The phase grown in epitaxy was also recently studied by STM [28] and X-ray absorption spectroscopy [15]. Another surface, also studied by LEED, was prepared from α-Fe_2O_3 faces by Ar^+ bombardment and subsequent annealing under oxygen pressure [17,18]; the reduction of the surface leads to the formation of a Fe_3O_4 (111) layer. The surface for the STM study [27] was a sample of natural crystal, cut and polished. Although the different preparation methods yield similar periodicities in LEED and similar STM patterns, there are differences in the structural conclusions reached by the different studies. The dynamical LEED analysis favors a surface terminating in a single Fe monolayer; the multiple scattering PD analysis favors a termination in an O layer without Fe, and the visual STM interpretation is a surface termination in two Fe monolayers. According to the LEED analysis, the three terminations have Pendry *R*-factors of 0.34, 0.5 and 0.5, respectively, indicating a clear LEED preference for the first structure.

In this paper, we present the results of ab-initio periodic Hartree–Fock calculations for the different structures of the (111) surfaces of Fe_3O_4 (magnetite). These calculations provide information about the energy of the unrelaxed and the relaxed surfaces and focus on the reasons why one termination is more stable than the others. We first investigated the termination by a single iron monolayer by varying many different geometrical parameters. The LEED results, first to be published, were indeed consistent with a large relaxation that we tried to reproduce from model calculations retaining the stoichiometry or, for extended systems, retaining at least the oxidation states that the ions have in the bulk. The main features derived from the experimental results are as follows: the interlayer distances at the surface differ drastically from those in the bulk; in the outermost oxygen sublayer, the atoms buckle into two separated monolayers. We next investigate other models allowing for deviations from the bulk stoichiometry and build systems with no dipole moment perpendicular to the surface. It will be shown that, based on our theory, the slab that terminates in iron bilayers on each side represents the energetically best compromise between proximity to the bulk stoichiometry and cancellation of the dipole moment. The termination by an iron bilayer would thus be the most favorable for the clean surface. Finally, we will show that the presence of hydrogen on the surface stabilizes the termination by a single iron monolayer and can explain the vertical displacements of the oxygen atoms observed in LEED experiments [18,25].

2. Computational aspects

2.1. Program and basis sets

Using the Hartree–Fock crystalline orbital program CRYSTAL [5], we performed effective-core pseudopotential calculations. The program describes crystalline solids at the ab-initio level by solving the Hartree–Fock equations. This program has also been extended to include a-posteriori density-functional corrections from Perdew (P91) [29] for the electronic correlation [30,31]. The application of these functionals is given in detail in Ref. [32]. The pseudopotentials come from Durand–Barthelat [33] and are listed in Table 1. For the iron atoms, we have modified the basis set from Durand–Barthelat by removing the most diffuse *d* function; it is indeed not possible to involve too diffuse functions in a periodic calculation since their superposition generates artefacts (linear dependency, etc.). The first four *d* functions were contracted as originally proposed while the exponent of the fifth and that of the sp orbital were optimized. We have determined two different basis sets for Fe^{2+} and Fe^{3+}. The basis set optimization was performed on the bulk structures assuming the experimental parameters [34]. For Fe^{2+}, we considered FeO in its low spin state (a restricted Hartree–Fock calculation). For Fe^{3+}, we considered the α-Fe_2O_3 oxide where Fe^{3+} is in a high spin state (an unrestricted Hartree–Fock calculation). In the iron oxides, the iron is cationic, and the population of the 4s and 4p orbitals is negligible. We have included a single gaussian to represent them and optimized the exponent. For oxygen atoms, we used the PS-31G basis set [35]. The exponent of the external orbital has been optimized ($\zeta = 0.252$); the orbital is then more diffuse than TiO_2($\zeta = 0.272$), which is less ionic.

In Sections 2–5, the geometric parameters (the spacing between the different layers) have been optimized 'by hand'. In Section 6, new results are presented using an automated optimization scheme using the steepest descent [36]. This procedure has allowed exchanges in the ordering of the layers that we did not permit for the initial successive optimizations of the parameters.

2.2. Tests on the FeO and Fe_2O_3 bulk structures

In this section, we present the results for the optimization of the bulk structures of the various oxides with the basis sets (Table 1) and compare them to experimental values. The lattice parameters are close to experimental values (Table 2). The optimization that includes the density-functional corrections P91 [29] does not significantly improve the description.

Table 1
Iron pseudopotentials and basis sets[a]

Fe pseudopotentials	APOT	CPOT	NPOT
P0	1.7842542	29.9870	0
P1	1.28775	19.69752	0
P2	2.92938	−12.11916	−1
P2	2.92938	−24.39136	2
	2.92938	17.49776	−1
Atomic orbitals of Fe	**Exponent**	**Coefficient**	**Coefficient**
4 sp	0.96	1.00	1.00
3 d	21.693742	0.070869	
	6.528837	0.239360	
	2.254905	0.447715	
	0.779185	0.393666	
3d′	0.25	1.00	

[a] The form of the radial function of the pseudo potential [35] is $\sum_{i}^{n} \mathrm{CPOT}\exp(-\mathrm{APOT}\ r^2) r^{\mathrm{NPOT}}$.

Table 2
Lattice parameters (Å) and cohesive energies, E_{coh} (defined positive, in kcal/mol), for different stoichiometries and spin arrangements[a]

	SCF	Perdew 91	Experiment
FeO	$a=4.25$ Å	$a=4.15$ Å	$a=4.30$ Å
	$E_{coh}=228.8$	$E_{coh}=252.0$	$E_{coh}=220.2$
α-Fe_2O_3 (antiferro)	$a=5.51$ Å	$a=5.39$ Å	$a=5.4135$ Å
	$\alpha=55°5'$	$\alpha=55°4'$	$\alpha=55°17'$
	$u(O)=0.550$	$u(O)=0.550$	$u(O)=0.550$
	$u(Fe)=0.355$	$u(Fe)=0.355$	$u(Fe)=0.355$
	$E_{coh}=708.8$	$E_{coh}=709.8$	$E_{coh}=570.8$
α-Fe_2O_3 (ferro)	$a=5.51$ Å	$a=5.408$ Å	
	$\alpha=55°5'$	$\alpha=55°4'$	
	$u(O)=0.55$	$u(O)=0.550$	
	$u(Fe)=0.355$	$u(Fe)=0.355$	
	$E_{coh}=708.0$	$E_{coh}=365.8$	
Fe_3O_4 ($n_\alpha-n_\beta=28$)	$a=8.54$ Å	$a=8.50$ Å	$a=8.39$ Å
	$u=0.380$	$u=0.380$	$u=0.379$
	$E_{coh}=956.2$	$E_{coh}=946.6$	$E_{coh}=798.3$
Fe_3O_4 ($n_\alpha-n_\beta=8$)	$a=8.54$ Å	$a=8.37$ Å	
	$u=0.381$	$u=0.382$	
	$E_{coh}=929.3$	$E_{coh}=927.0$	

[a] Experimental values are derived from Ref. [44]: $\Delta H_f^\circ(FeO)=-63.2$ kcal/mol, $\Delta H_f^\circ(Fe_2O_3)=-196.56$ kcal/mol; $\Delta H_f^\circ(Fe_3O_4)=-267.1$ kcal/mol; $\Delta H_f^\circ(Fe_g=96.68$ kcal/mol), $E_{dissociation}$ $(O_2)=120.6$ kcal/mol [60]. The calculated atomic references for the iron atoms (^{5}D state) are -21.128 a.u (HF) and -21.278 a.u. (P91).

Cohesive energies are also displayed in Table 2. The basis set that we have determined for a good description of the oxide is not adequate for the ground state of the iron atom (^{5}D, d^6s^2) since the representation of the 4s orbital is too minimal. The cohesive energies are therefore overestimated. To determine the cohesive energies with this basis set, we have located the ground state 0.150 a.u. below the calculated (^{3}F, d^8) state as it is experimentally [37,38]. Then, the cohesive energies appear to be reasonable.

FeO (wüstite) crystallizes in the rocksalt structure [34]. The geometry optimization leads to a lattice parameter shorter than the experimental one (see Table 2).

α-Fe_2O_3 (hematite) crystallizes in the corundum structure (space group R-3C), with hexagonal close packed layers of oxygen atoms and two-thirds of octahedral holes in between filled by Fe^{3+} ions. The crystal is described by the rhombohedral lattice parameter, $a=\sqrt{11/3}d_{OO}$. It can also be viewed as being composed of 'sandwich' trilayers, each being a monolayer of oxygen atoms in between two layers of iron, stacked along the c′ direction of an hexagonal lattice. When the structure is perfect, the correspondence between the rhombohedral and the hexagonal parameters is given by $a'=3a/\sqrt{11}$ and $c'=a\sqrt{72/11}$. The experimental structure is slightly distorted: the parameters α, u(Fe) and u(O) deviate from their values in the perfect packing, $\alpha=53°47$, $u(Fe)=1/3$ and $u(O)=7/12$. Our optimized geometric parameters (Table 2) are in good agreement with the experimental values as already found [39,40] with other basis sets.

Below the Néel temperature, $T_N=953$ K, the stable phase is antiferromagnetic; the Fe ions within the same monolayer have the same spin, opposite to those of adjacent layers. The stable magnetic structure corresponds to a $Fe(\alpha)O_3Fe(\beta)Fe(\beta)O_3Fe(\alpha)$ spin sequence on the four successive Fe atoms along the threefold axis [41]; the symmetry is lowered to R-3. We also calculated a hypothetical ferromagnetic structure that would correspond to the R-3C symmetry having four Fe atoms with spin up. We found this

structure to be slightly less stable (by 1–5 kcal/mol) than the antiferromagnetic structure in agreement with observed magnetism; this is comparable to results obtained with larger basis sets [22].

3. Fe_3O_4 (magnetite)

3.1. Bulk

Fe_3O_4 (magnetite) has the inverse spinel structure [34], in which the Fe cations occupy interstices of the fcc close packed frame of O^{2-} ions. The primitive cell of Fe_3O_4 contains six Fe atoms. It is a mixed-valency compound [42,43], with two Fe^{3+} ions per primitive cell (eight Fe^{3+} ions per cubic cell) in tetrahedral sites and four ions (two Fe^{3+} and two Fe^{2+}) in octahedral sites. Below 119 K, the electrons are trapped in a site, and the magnetite is an insulator. Above this temperature ('Verwey transition'), this magnetite is a good conductor, and its good conductivity is caused by a rapid hopping of electrons between Fe^{3+} and Fe^{2+} ions in octahedral sites, resulting in a mean oxidation number of 2.5 for these ions (Fig. 2) [43]. Thus, the system has a high spin with a large excess of electrons of spin up: $n_\alpha - n_\beta = 18 \pm 10$ per unit cell, depending on the spin orientation of the Fe^{3+} ions that occupy the tetrahedral sites. The stable phase is ferromagnetic with $n_\alpha - n_\beta = 28$. The optimized geometric parameters are in reasonable agreement with experiment (Table 2). The P91 correction does not improve the cohesive energy. On the contrary, the disproportionation reaction, which is nearly athermic (−7.4 kcal/mol [44]), is calculated to be slightly endothermic when the correction is made. The DOS is represented in Fig. 3. The 2p(O) levels are at ~15 eV below the Fermi level, which corresponds to a low fraction of the β spinorbitals localized on the iron in octahedral sites; the system is found to be metallic. The calculation therefore simulates the high-temperature metallic phase of magnetite.

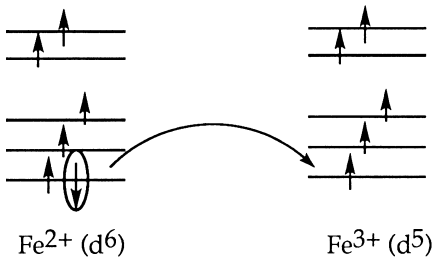

Fig. 2. Exchange mechanism giving ferromagnetic coupling between Fe^{2+} and Fe^{3+}, depicted in an atomic energy level diagram. An electron of minority spin (β) is transferred from an ion in an octahedral position with five valence electrons of α spin to another.

3.2. Fe_3O_4 (111) surface

The (111) orientation corresponds to a stacking of layers as shown in Fig. 4. A top view is shown in Fig. 5. The iron layers (dense monolayers or multilayers) alternate with the oxygen layers. The latter are close packed layers that are the most dense layers in fcc lattices, whereas the former are incomplete layers, a 'hole' corresponding to the fourth site. Dense monolayers of iron involve only atoms in octahedral sites, all in essentially the same plane midway between oxygen layers. By contrast, the multilayers involve iron atoms in tetrahedral sites, closer to the basal plane than to the apical plane (a quarter of the distance between two oxygen layers) and iron atoms in octahedral sites midway between oxygen layers. Thus, the iron multilayer is a stacking of three distinct low-density monolayers. The iron atoms in tetrahedral sites of the first monolayer (closest to the dense layer) are directly above the 'hole' sites. The lattice parameter, u, deviates in the bulk from the ideal value, 0.375. The 4O monolayer, therefore, also splits into two monolayers, 0.04 Å apart. Figs. 4 and 6 show the resulting distinction between three O_B atoms and one O_A atom; they are connected differently to the tetrahedral atoms of the multilayer; for three O_B atoms, the [111] direction is a local C3 axis, whereas for the O_A atom, it represents a C2 axis; the O_A atom is connected to three atoms of the dense layer and the iron of the most distant monolayer that is directly above it. In the bulk, the layer that contains the O_B atoms is above (closer to the iron multilayer by 0.04 Å) that with the O_A atom. One of the main features of the surface relaxation derived from the LEED experi-

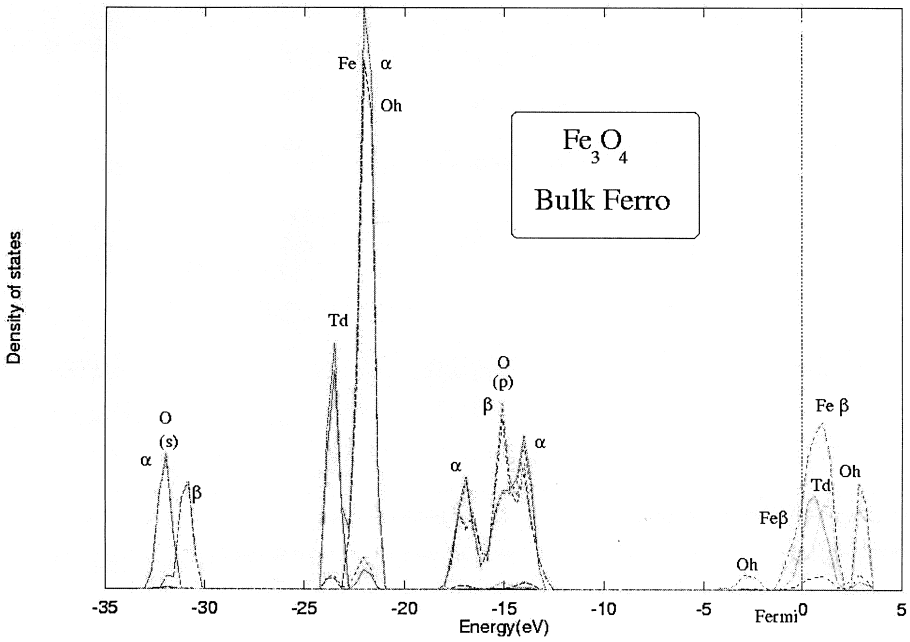

Fig. 3. Densities of states for the bulk Fe_3O_4 shows the metallicity and the ferromagnetism. The Fermi level lies close to the bottom of the iron levels with β-spin; it is mostly the density on the atoms in octahedral position that are below the Fermi level. The iron states with α-spin are at $-21/-24$ eV below the Fermi level. The 2p(O) levels are at $-13/-17$ eV below the Fermi level.

ment [25] is the upward displacement of the atom O_A. It is displaced above the plane of the O_B atoms, and the interlayer spacing changes from -0.04 Å in the bulk to 0.40 Å in the surface [25].

The alternation of charged layers (positive: monolayers or multilayers of ferrous and ferric ions; negative: layers of O^{2-}) generates an instability when they are regularly paired: each pair (cation layer plus anion layer) has a dipole moment and acts like a capacitor [4,45]. The repeat of the pair generates a series of capacitors. Then, the potential of each ion diverges linearly. Such a system reconstructs or relaxes at the surface to decrease the dipole moment by strong variations of the interlayer spacings. This concerns (111) faces of NiO [46], MgO [47,48] and CaO [42]: the variations in the interlayer spacings [49] exceed 15%, whereas the non-polar faces maintain the bulk structure within the experimental uncertainty (5%). There are also other modes for the reconstruction. The surface can alternatively facet to generate non-polar surfaces [45,47,48]. The surface atoms may change their oxidation state and become neutral so as to reduce the dipole moment [50]. The hydroxylation is a way to oxidize the oxygen dianions [51]. The dipole moment can vanish by an additional monolayer on one side; then, the opposite faces of the crystal have the same charge [45,51].

In the present investigation, the Fe_3O_4 (111) surface is modelled by a slab. The two-dimensional unit cell is represented in Figs. 4 and 5. We assume complete layers [we did not consider models that remove an oxygen from the 4O layer or an iron atom from the 3Fe(Oh) layer]. Then, six possible terminations for the Fe_3O_4 (111) surface result from the bulk truncation and are investigated here; these are shown in Fig. 7.

4. Models respecting the bulk stoichiometry

We first assume that the cleavage does not modify the oxidation states of the atoms for the following reasons: the 2p(O) levels are low in energy, making the oxidation of the oxygen ions

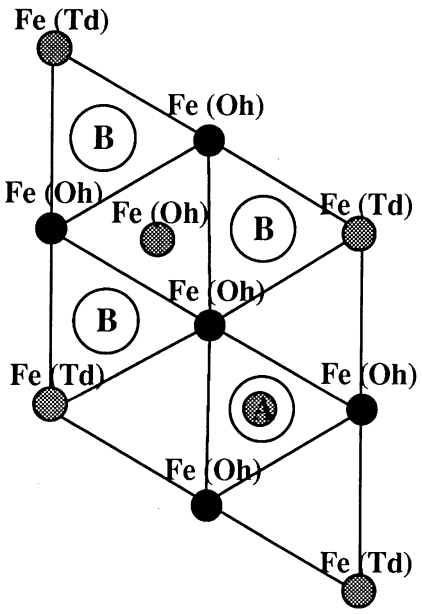

Fig. 4. Frame showing the unit cell linking iron atoms in tetrahedral positions. In the dense layer that contains three iron atoms in octahedral positions (black circles), the origin appears to be a vacant site ('hole' site). Above this plane, the four oxygen atoms are represented by white circles; when $\Delta_2 < O$, the O_A atom is below the O_B atoms (closer to the dense layer); this is the situation for the bulk; when $\Delta_2 > O$, it is the opposite; this situation is predicted from the LEED calculations [25]. Next above, the multilayer of three iron atoms is represented by gray circles: the Fe site (Td) at the origin lies in the lowest layer; in the intermediate layer, the Fe site (Oh) is above the center of symmetry between the three O_B atoms; in the superior layer, another Fe site (Td) is right above the O_A atom. Beneath the dense layer (black circles), a similar pattern not represented would be obtained through a symmetrical inversion relative to the central site (see oxygen atoms labelled A, B, C and D in Fig. 5).

unlikely; −II is the ordinary oxidation state of the oxygen atom, and the negative electron affinity of O^-, −9 eV, is compensated by the Madelung field. Concerning the iron atoms, standard oxidation states are II (ferrous) and III (ferric), and the large ionization potential for Fe^{3+}, 56.7 eV, prevents the formation of Fe^{4+}. In the absence of oxidative–reductive processes (by adsorption or by compensation for instance on the opposite face), oxidation numbers remain the same, and then neutrality imposes the stoichiometry.

We choose a six-layer slab model with stoichiometry Fe_6O_8 since it contains one 'repeat unit' perpendicular to the (111) surface. The slab model represents a thin film at the surface region. It is smaller than the experimental Fe_3O_4 film obtained by deposition onto Pt [18,25] (each successive deposition and oxidation of eight monolayers of iron should generate one dense layer of iron). For the ferromagnetic species, there are six ferrous ions and four ferric ions; this leads to 28 more α electrons than β electrons.

The opposite terminations of each stoichiometric slab are coupled; the slabs are restricted to six layers and the bulk layer sequence. The termination by one iron layer is coupled with that by two iron layers. The termination by an oxygen layer is coupled with that by three iron layers (an iron multilayer or a dense layer using the terminology used in Fig. 1).

4.1. Two best terminations resulting from an ideal cleavage

A cleavage through the iron multilayer can generate two terminations consisting of one and two iron monolayers, respectively. This is clearly the most favourable cleavage since it only breaks five bonds (two short and three long) against seven or nine for the cleavages between one oxygen layer and one iron layer (dense monolayer or multilayer). Considering only cuts made of complete layers, this slab also represents the least polar cut: the cleavage through the multilayer generates iron terminations on both sides of the slab. The optimal possibility leading to a non-polar cut would be obtained by the cleavage of a monolayer: the termination by an incomplete layer on each side. This would double the unit cell for the slab periodicity and would be seen by LEED.

The relative energies of the unrelaxed slab reveal very large differences, supporting this analysis (Table 3). The termination by one iron layer proposed on the grounds of LEED determination and that by two iron layers supported by STM visualization both emerge from this simple analysis. These models should be differentiated by an analysis of the extent of the relaxation or by considering non-stoichiometric models.

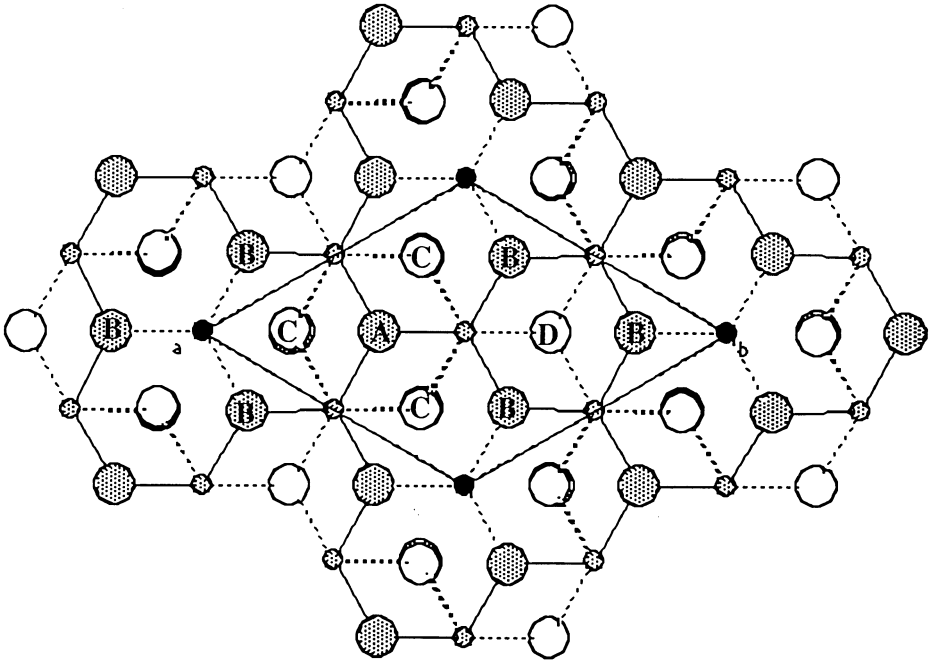

Fig. 5. Top view of an ideal bulk termination of the (111) Fe_3O_4 surface. Oxygen anions are indicated by large open and gray circles labelled A, B, C and D. The iron cations are represented by small circles (the black ones represent the irons in tetrahedral positions, the gray ones in the octahedral positions). The two dimensional unit cell is also shown. In reality, we should note that the four atoms $O_A(O_D)$ and $O_B(O_C)$ are not exactly close packed in the spinel structure but are slightly buckled out of coplanarity. The real Fe_3O_4 parameter, $u=0.379$, differs from the value in the perfect close packed lattice of oxygen atoms, $u=0.375$.

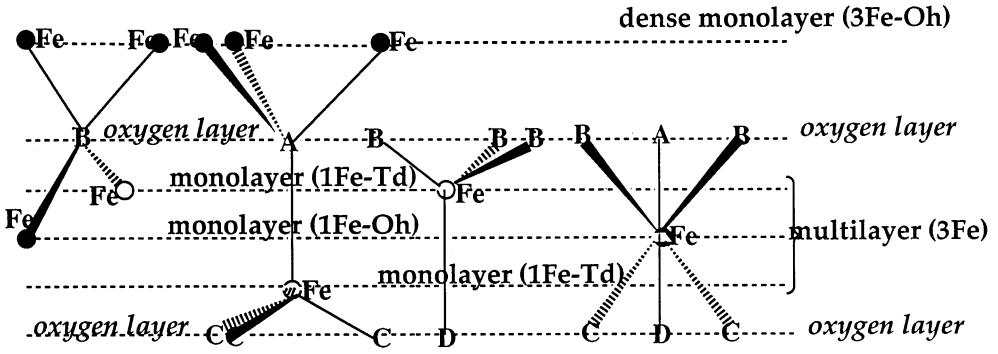

Fig. 6. Coordination of the different atoms in the Fe_3O_4 (111) slab. For the O_A atoms, the [111] direction is a local C_3 axis while it is a local C_2 axis for the O_B atoms. The O_A are threefold-coordinated to the dense layer and singly coordinated to the most distant layer from the multilayer; the O_B atoms are twofold-coordinated to the dense layer and coordinated to the two closest layers from the multilayer. In the ideal structure, the spacing between the layers that belong to the multilayer represents one-quarter of the spacing between two oxygen layers.

4.2. Relaxations in the stoichiometric models

In this section, we investigate the relaxations derived by LEED, in particular the finding of opposite buckling (compared to the bulk) in the oxygen layers that contain O_A and O_B. The two faces of the Fe_6O_8 slab can represent both the termination by one iron monolayer and the ter-

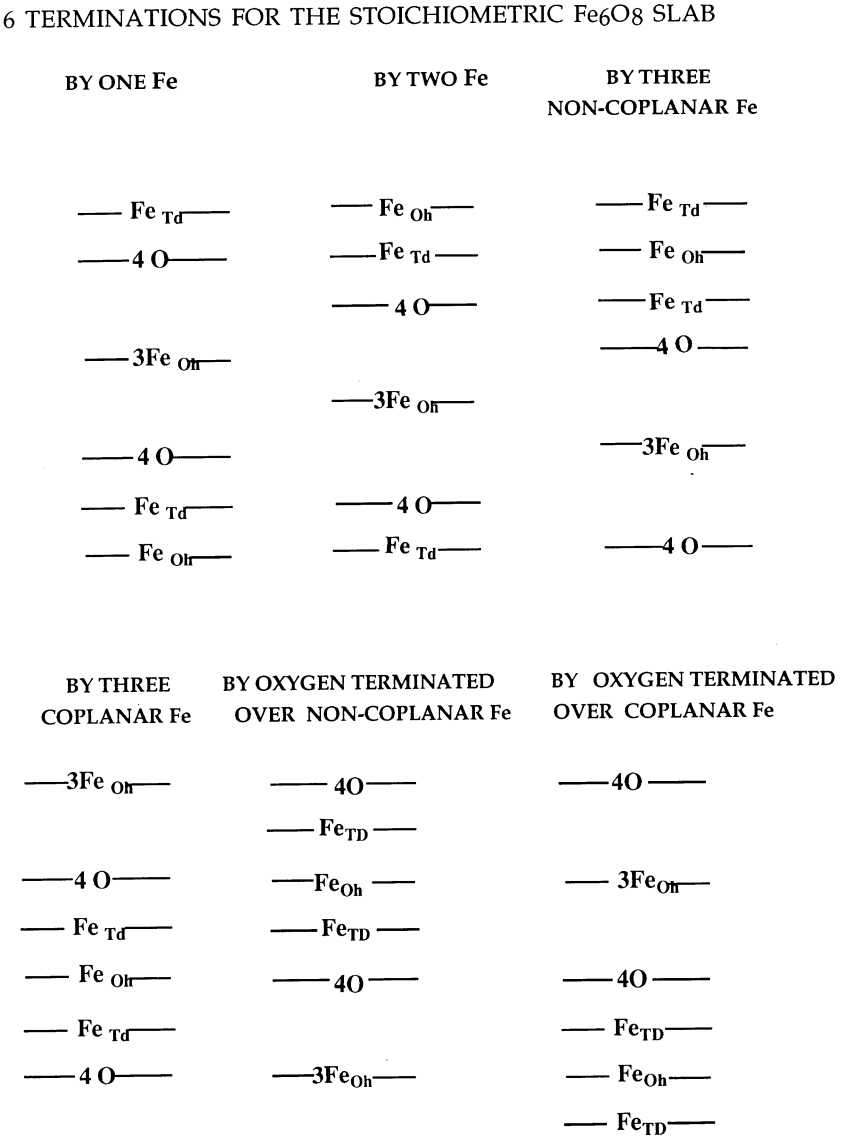

Fig. 7. Six possible bulk-like terminations of the Fe_3O_4 (111) slab.

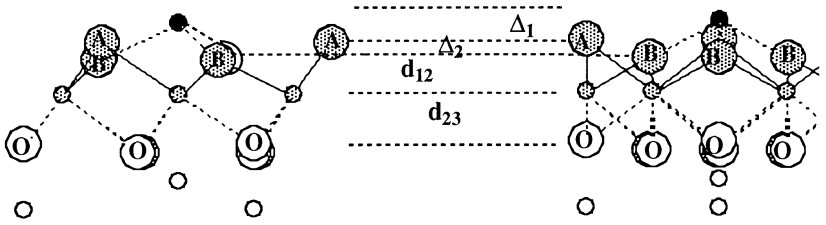

Fig. 8. Two (mutually perpendicular) views parallel to the surfaces of a Fe_6O_8 slab, showing interlayer spacings involved in the relaxation at the face terminated by a single Fe monolayer. Large (small) circles represent O (Fe) atoms.

Table 3
Number of broken bonds generated by three different cleavages and relative energies for the unrelaxed slabs resulting from those cleavages

Sequence of the stoichiometric slabs generated by the cleavages	Number of broken bonds	Relative energy (kcal/mol)
$Fe_{Td}O_43Fe_{Oh}O_4Fe_{Td}Fe_{Oh}$	5	0.0
$O_43Fe_{Oh}O_4Fe_{Td}Fe_{Oh}Fe_{Td}$	7	+247.2
$O_4Fe_{Td}Fe_{Oh}Fe_{Td}O_43Fe_{Oh}$	9	+361.5

mination by two iron monolayers. However, since experiment observes a single face (let us call it the 'top' face), the 'bottom' face is initially assumed to represent the atoms in the bulk; so, at first, the bottom atoms were kept at fixed positions. In addition, the complete relaxation of the slab implies the optimization of many parameters, and we had to vary them independently; the variation is, in practice, not independent of the order of optimization, and we had to do it iteratively. Computational constraints limited the number of adjustable parameters. We have optimized four on the basis of the LEED results, namely those labelled Δ_1, Δ_2, d_{12} and d_{23}, in Fig. 8. In so doing, we restrict ourselves to the study of the relaxation for the termination by a single iron layer.

The results are summarized in Tables 4 and 5. The former expresses the values of interlayer spacings that are conveniently compared with experiment; the latter gives the bond distances and should be more physical. Indeed, since the surface Fe atoms are bound to the atoms O_B, a variation of the bond modifies $\Delta_1+\Delta_2$, which are defined in Fig. 8. Table 5 shows that the bond lengths do not vary by much, and this explains why the parameters that define the relaxation of the slab are not really independent. This remains close to the situation in the bulk and does not agree with the LEED results. The results obtained with the UHF Hamiltonian differ from those proposed from Ref. [25]. In particular, the O_B atoms are closer to the surface than the O_A atoms (Δ_2 is even more negative than in the bulk). We also tested several variations, such as allowing displacements in the plane, which did not, however, bring the parameters closer to experiment. Finally, we have increased the thickness of the slab, and we have saturated the 'bottom' layer, to avoid modifying the oxidation number of the atoms. The O_B atoms are saturated by hydrogen atoms, and the O_A atom is saturated by a Zn atom (at the position where the tetrahedral iron should be); the Zn atoms, as Zn^{2+}, allow the appropriate electron count, and their ionic radius is close to that of the ferrous ion. This results in a $Fe_7O_{12}H_3Zn$ slab; UHF calculations on this model lead again to relaxations that are similar to those of Table 4.

Table 4
Surface relaxations (Å) for the stoichiometric Fe_6O_8 slab for a termination by one iron monolayer (see text for details)

	RHF	UHF	P91	UHF saturated	Exp. LEED [25]	Bulk [34]
Δ_1	0.47	0.54	0.54	0.55	0.40	0.626
Δ_2	0.36	−0.08	−0.08	−0.10	0.42	−0.04
d_{12}	0.98	0.90	0.90	1.00	0.83	1.193
d_{23}	1.40	1.39	1.29	1.40	1.42	1.193

Table 5
Calculated and experimental [25,34] Fe−O distances (Å) for the bulk and the Fe_6O_8 slab for a termination by one iron monolayer

Bonds	Bulk		Surface	
	Calculation	Experiment	Calculation	Experiment
$Fe_{Td}-O_3$	1.92	1.88	1.80	1.98
$Fe_{Oh}-O_1$	2.09	2.07	1.90	2.12
$Fe_{Oh}-O_3$	2.09	2.07	1.93	1.87

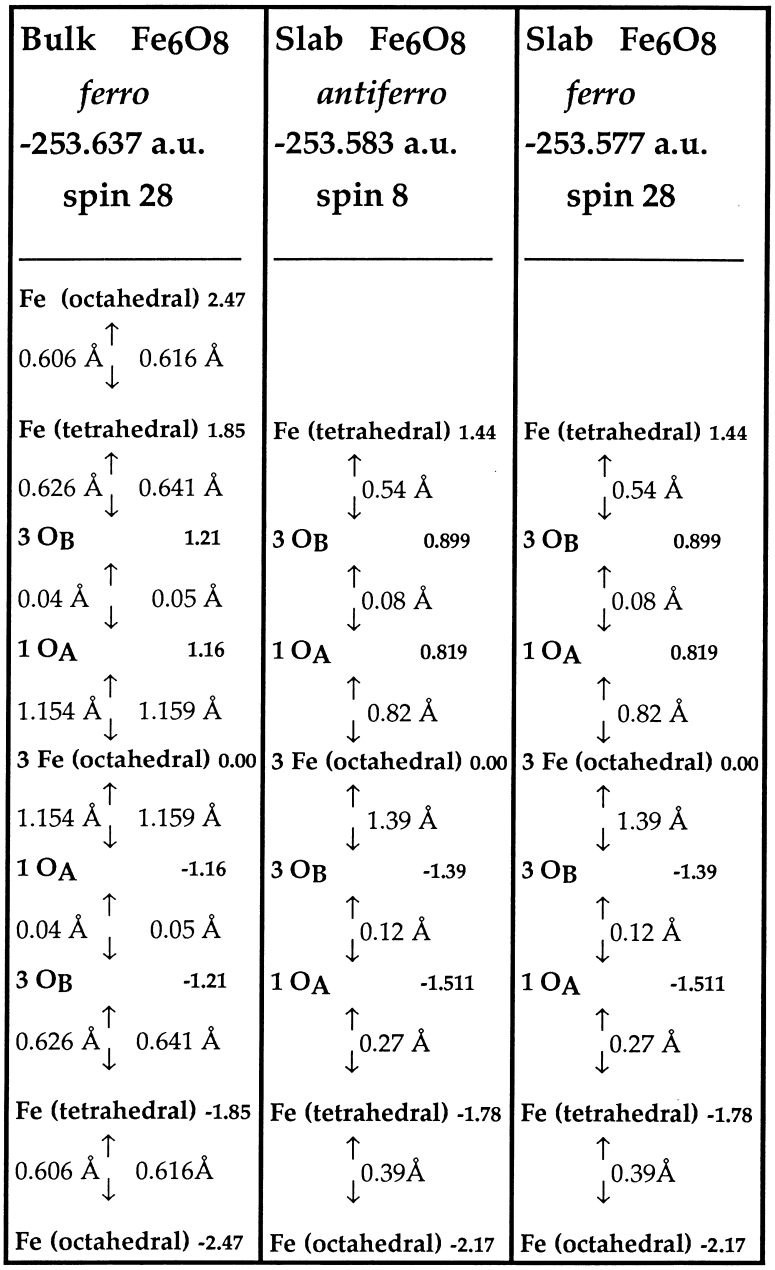

Fig. 9. Optimized calculated interlayer spacings for the Fe_6O_8 relaxed slab, compared with the bulk values (experimental [34] on the left-hand side, and calculated on the right-hand side). The presentation of the figure follows the ordering of the successive layers and is that shown in Fig. 7 (termination by one or two iron layers). The optimization of the parameters has been made sequentially on the antiferromagnetic slab; except for O_A vs. O_B, no reordering of the layer has been considered. The relaxation reduces the difference between the center of mass for the positive and negative charges (0.044 Å, calculated using the Mulliken charges). The height relative to the central layer (the dense layer of octahedral iron atoms) is indicated in angstroms.

The optimization of both faces of the Fe_6O_8 slab improves its cohesive energy to 84.8% of that of the bulk. The middle column in Fig. 9 shows the resulting relaxations of the interlayer spacings for the two faces (face up with one iron monolayer and face down with two Fe). The center of mass of the oxygen layers is pushed down (toward the face with two iron monolayers) to decrease the vertical dipole moment. The distance between the two iron layers at the bottom surface (see Fig. 9) is half that of the bulk. This may be explained by simple arguments: the coordination of the iron atoms in the two surface layers is 3 in both cases, and we can expect them to reside above the oxygen layer at more or less the same height. The interstitial sites in the bulk impose a distinction that disappears with the cleavage.

5. Models deviating from the bulk stoichiometry

5.1. Symmetric models

So far, we have imposed the bulk stoichiometry and hoped that the relaxations would contribute to decrease the dipole moment with no modification of the oxidation states of the atoms. Another approach involves imposing a symmetry between the layers to cancel the net dipole moment of the entire slab by symmetry. If the slab is centered on one monolayer (we assumed a dense monolayer with octahedral iron atoms), we could generate such a slab. There is another advantage in imposing a symmetry; the two terminations are then identical, and a slab is associated with a single termination. Thus, the Fe_5O_8 slab corresponds to the termination by a single iron layer and the Fe_7O_8 slab to the termination by two iron monolayers. We have optimized the interlayer distances for these two slabs, and the results are displayed in Fig. 10, adding for comparison an intermediate non-symmetrical slab, Fe_6O_8.

The progression from Fe_5O_8 to Fe_6O_8 and next to Fe_7O_8 or beyond can be considered as the sequential adsorption of monolayers of iron. Each additional monolayer corresponds to adsorbing on a threefold site and building three Fe—O bonds (except beyond Fe_7O_8; a unique bond is formed for a top site adsorption). The stability of the slab can thus be viewed as a problem of adsorption; the most stable termination corresponds to the saturation for the surface.

Before looking at the results of the calculations, let us consider the situation from the point of view of the deviation of the stoichiometry. The oxidation state for the iron ion must be between II (ferrous) and III (ferric). The averaged oxidation states for the slabs are, respectively, 3.2, 2.6 and 2.28. This means that the Fe_5O_8 slab (and the termination by a single iron layer) is unlikely. The fourth potential ionization for iron, 56.8 eV, is too high to generate an Fe(IV) ion necessary to give the averaged state of 3.2. Even if all the iron were in oxidation state +III, some oxygen atoms should be reduced to −I. This does not happen except when two oxygen atoms are bound to each other. It should be very difficult to remove the electrons from the oxygen centers. The Fe_5O_8 slab is Fe-deficient; there are not enough electrons available to be transferred to the oxygen atoms to make them O^{2-}. When there are defects in the metal oxide, they are usually O-deficient. (See, for example, the ratio between Ti and O in TiO_2 [52–55]. O deficiency also occurs in SnO_2 [56], $SrTiO_3$ [57] and Al_2O_3 [58]. On MgO(111), Pojani et al. have shown that it is easier to remove a surface oxygen layer than a magnesium layer [51]). Metal vacancies are obtained for metal oxides with low oxidation states; then, the vacancy is accompanied by an increase of the oxidation state of a remaining metal atom (Ti vacancies in TiO). For the bulk, non-stoichiometric magnetite is obtained by further oxidation of ferrous ions to ferric, accompanied by vacancies distributed randomly over the octahedral sites [43]. Iron-deficient magnetite surfaces have been grown epitaxially onto MgO(100) [43]. The Fe_5O_8 slab model would go beyond the limit, imposing, in addition to the complete oxidation to ferric species, the reduction of an oxygen dianion. The Fe_7O_8 slab appears to be much more reasonable. In the Fe_7O_8 slab, the iron atoms in the tetrahedral sites are ferric as they are in the bulk, and all the iron atoms in the octahedral sites are ferrous (half of them are ferrous, and half of them ferric, for the Fe_3O_4 stoichiometry).

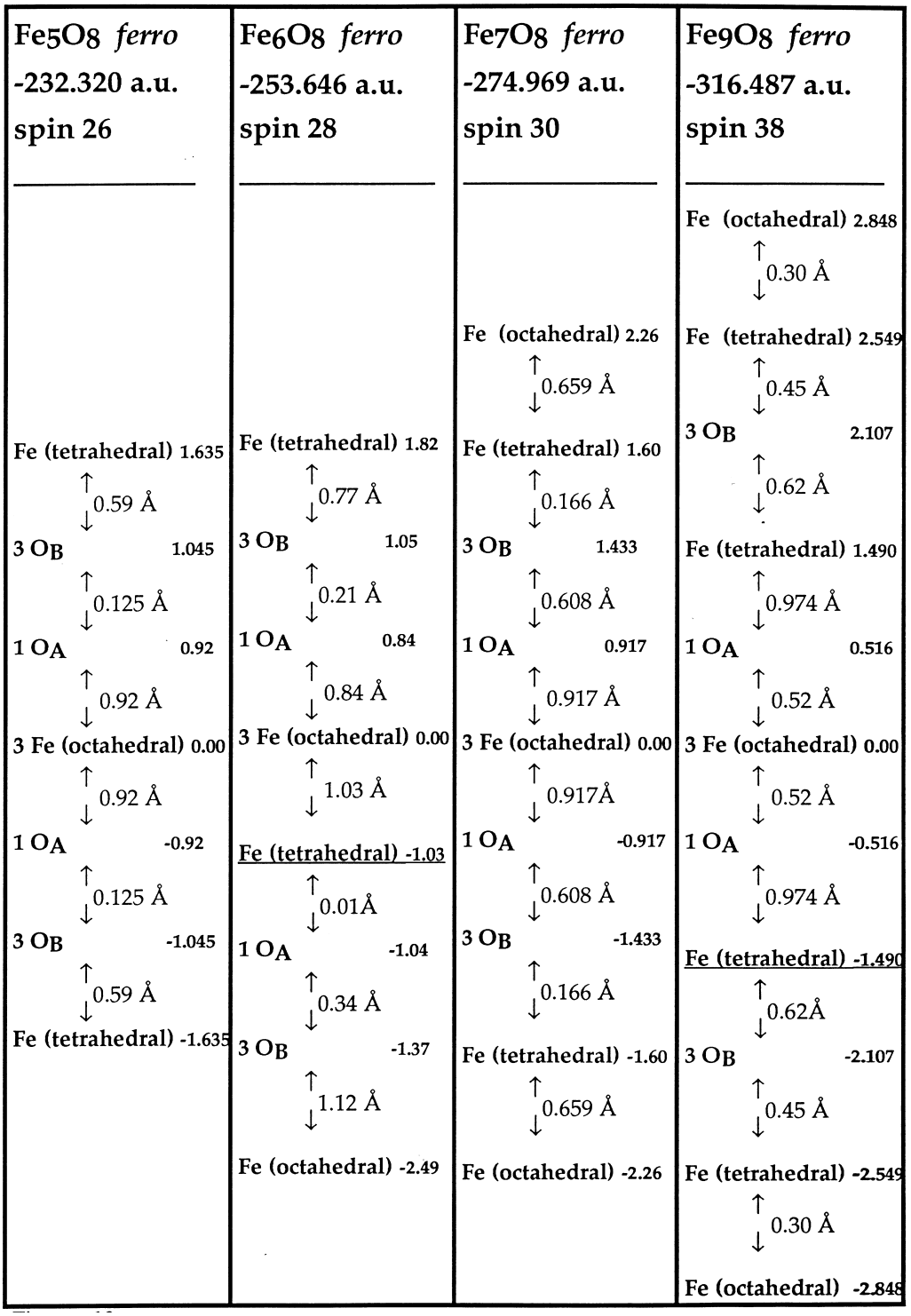
Fe5O8 ferro
-232.320 a.u.
spin 26
Fe (tetrahedral) 1.635
0.59 Å
3 OB 1.045
0.125 Å
1 OA 0.92
0.92 Å
3 Fe (octahedral) 0.00
0.92 Å
1 OA -0.92
0.125 Å
3 OB -1.045
0.59 Å
Fe (tetrahedral) -1.635
Fe6O8 ferro
-253.646 a.u.
spin 28
Fe (tetrahedral) 1.82
0.77 Å
3 OB 1.05
0.21 Å
1 OA 0.84
0.84 Å
3 Fe (octahedral) 0.00
1.03 Å
Fe (tetrahedral) -1.03
0.01Å
1 OA -1.04
0.34 Å
3 OB -1.37
1.12 Å
Fe (octahedral) -2.49
Fe7O8 ferro
-274.969 a.u.
spin 30
Fe (octahedral) 2.26
0.659 Å
Fe (tetrahedral) 1.60
0.166 Å
3 OB 1.433
0.608 Å
1 OA 0.917
0.917 Å
3 Fe (octahedral) 0.00
0.917Å
1 OA -0.917
0.608 Å
3 OB -1.433
0.166 Å
Fe (tetrahedral) -1.60
0.659 Å
Fe (octahedral) -2.26
Fe9O8 ferro
-316.487 a.u.
spin 38
Fe (octahedral) 2.848
0.30 Å
Fe (tetrahedral) 2.549
0.45 Å
3 OB 2.107
0.62 Å
Fe (tetrahedral) 1.490
0.974 Å
1 OA 0.516
0.52 Å
3 Fe (octahedral) 0.00
0.52 Å
1 OA -0.516
0.974 Å
Fe (tetrahedral) -1.490
0.62Å
3 OB -2.107
0.45 Å
Fe (tetrahedral) -2.549
0.30 Å
Fe (octahedral) -2.848

Fig. 10a.

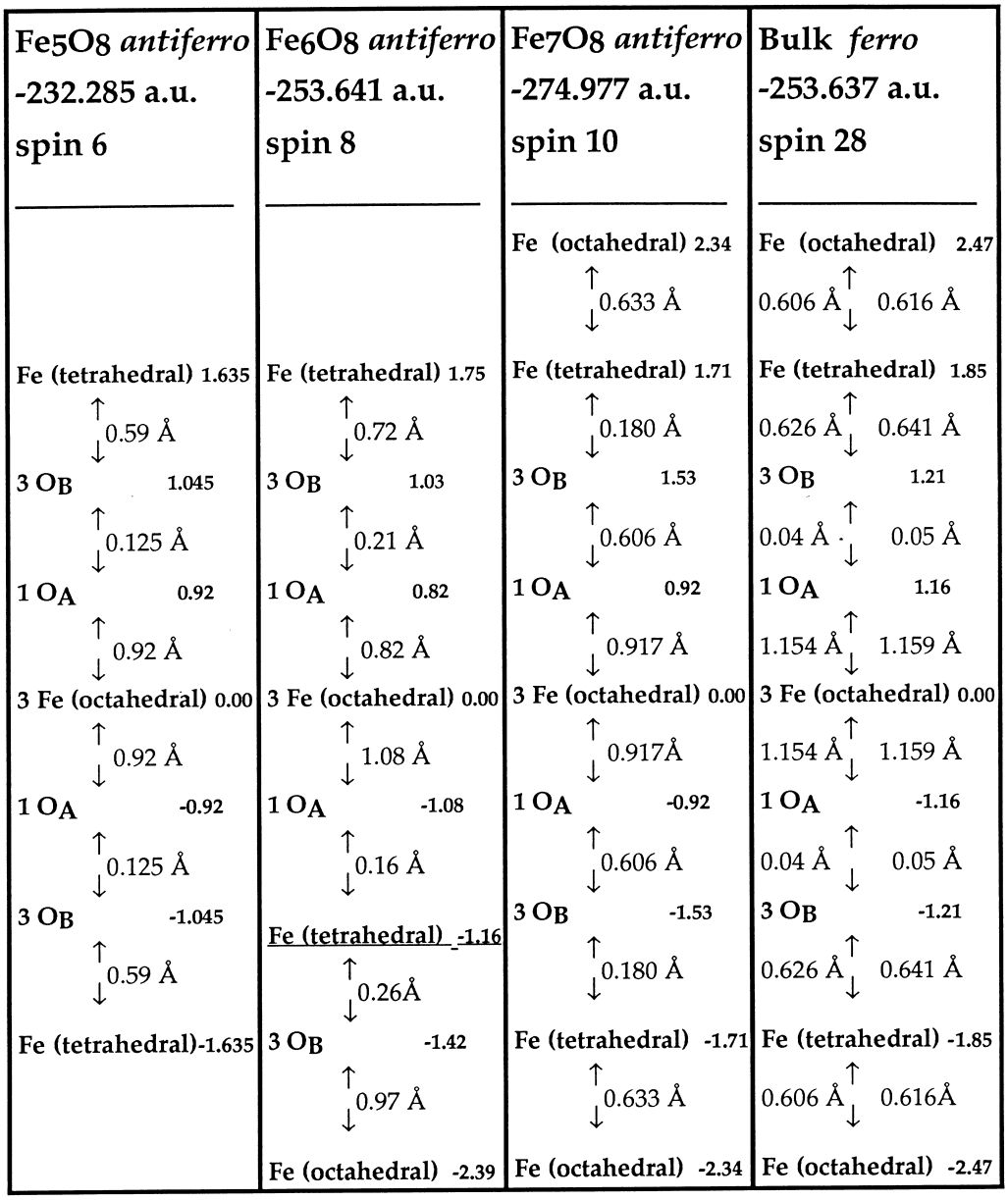

Fig. 10b.

Fig. 10. Optimized calculated interlayer spacings for relaxed slabs for the ferromagnetic cases (Fig. 8a) and the antiferromagnetic case (Fig. 8b, three rightmost columns) compared with the bulk experimental values [34]. The height relative to the central layer (the dense layer of octahedral iron atoms) is indicated in angstroms. Layers that are switched (with a different ordering from that of the bulk) are underlined.

The energies and the geometries of the various slabs are presented in Fig. 10a (ferromagnetic cases) and Fig. 10b (antiferromagnetic cases). For the antiferromagnetic state, we have considered that all the electrons of the octahedral sites have alpha spins (allowing electron hopping from one

site to another), whereas those of the tetrahedral sites have beta spins. From here on, we will retain the result of the lowest energy; except for the Fe_5O_8 slab that is the least realistic model, the most stable systems are ferromagnetic. The simultaneous optimization of several interlayer spacings has been performed using the steepest descent method (Section 2.1).

The complete optimization of the Fe_6O_8 slab improves its cohesive energy by 85 kcal/mol (the cohesive energy for the slab reaches 86.9% of that of the bulk). The main variation is a switch between two layers in the bottom side (the surface ending normally by two iron layers). The layer with tetrahedral iron atoms exchanges its sequence with that of the O_B atoms. Then, the iron atoms at the origin of the cell (Fig. 4) move close to the empty space of the dense layer. This switch doubles the improvement in energy due to the simple relaxation. There is no switch for the Fe_7O_8 slab, which, nevertheless, appears to have a very large cohesive energy.

The sequence of successive adsorption energies of the monolayers is as follows:

$$Fe_5O_8 \overset{-40.7\ \text{kcal/mol}}{\rightarrow} Fe_6O_8 \overset{-44.1\ \text{kcal/mol}}{\rightarrow} Fe_7O_8 \overset{+634.8\ \text{kcal/mol}}{\rightarrow\rightarrow} Fe_9O_8.$$

The first two steps are exothermic. The symmetric slabs appear more favorable than Fe_6O_8, the stoichiometric slab (adding the seventh layer and losing the stoichiometry is more exothermic than adding the sixth iron layer). The Fe_7O_8 slab represents the saturation; to prove this, we have calculated the symmetric slab Fe_9O_8, terminated by two complete multilayers. Because of the symmetry, this slab also has no net dipole moment. There are two switches for the Fe_9O_8 slab which do not significantly improve the cohesive energy. Note that the iron layer that moves inward remains distant (1.49 Å) to the dense layer of iron. The addition of the two last layers is strongly endothermic. At this stage, the model that seems most favorable is the Fe_7O_8 slab.

5.2. Relaxation of the Fe_7O_8 slab

The relaxations for the Fe_7O_8 slab lead to a compression of the outermost interlayer spacings; the thickness of the slab, 2.26–2.34 Å, is smaller than in the bulk, 2.47 Å. Atoms at the surface, whose coordination has been reduced relative to the bulk, move inward to strengthen their interaction with the atoms of the sublayer to which they are bound. This is the case for the O_A atoms and not for the O_B atoms that remain tetracoordinated. Consequently, the interlayer distance, Δ_2, increases from 0.04 Å in the bulk to 0.61 Å in the slabs. The atoms O_A have lost one bond and are singly bound to the dense iron layer. The shift toward this layer is large (1.16–0.92 Å); the bond distances decrease from 2.09 to 1.95 Å. The interlayer distance between the layer of the oxygen atoms O_B and the top layer (octahedral iron atoms) decreases from 1.25 to 0.8 Å. The Fe—O distances do not vary as dramatically as the interlayer spacings (from 2.09 to 1.905 Å). The interlayer distance between the layer of the oxygen atoms O_B and the second layer (tetrahedral iron atoms) decreases from 0.64 to 0.17 Å, corresponding to a reduction of the Fe—O distances from 1.93 to 1.72 Å. Since the coordination of the oxygen atoms O_B has not changed and since the binding with the surface layers increases, the binding with the iron layer beneath (three octahedral Fe of the dense layer) should decrease. This is indeed what is found (the spacing increases from 1.21 to 1.53 Å, and the Fe—O bond distances increase from 2.09 to 2.27 Å).

5.3. Possible switch of the layers in the Fe_7O_8 slab

The unrelaxed Fe_6O_8 slab presents two surfaces with terminations by one or two iron layers. After optimization, a switch occurs moving the Fe(Td) layer inward. The switch brings the tetrahedral atoms close to the dense layer, where it seems easy to locate a fourth iron atom. The switch increases the coordination of the Td atoms; if they completely reach the 'hole' site of the dense layer, they would become octahedral. It seems at first inconsistent that the termination of the bottom face of the Fe_6O_8 slab, with two iron layers, appears to be very different from that obtained for the Fe_7O_8 slab: there is a switch in the first case and not in the second case. This raises the question of the validity of the models. Our symmetric model

is certainly too small. It forbids the motion of the Fe(Td) layer from both sides since the atoms from the opposite sides would become too close to each other. To allow the switch without increasing the size of the slab, we must therefore break the symmetry, impose on one half (the lowest layers) the geometry of the bulk and optimize the interlayer spacings of the other side (the upper layers). As the bottom surface is not allowed to relax, we expect the values of the cohesive energies with this constraint to be inferior to those obtained with a symmetric slab. This is indeed what is obtained by calculations for the ferromagnetic case (see Fig. 11). We have obtained two minima on the energy surface. One without permutation, 89 kcal above the symmetric slab, and one with permutation, only 23.7 kcal above. This shows that the surface layer rearranges only if the deeper layers are fixed. In the real system, the deeper layers are freer to adapt than in the symmetric slab, where half of the slab is constrained to be identical to the other half. The antiferromagnetic case is not the ground state and does not lead to an inversion of the layers. Indeed, the inversion brings the atom of the second iron layer (initially ferric ions) near the hole of the dense layer (made of ferrous and ferric ions) and tends to form a complete layer with four equivalent atoms per unit cell. Then, the electron from the ferrous sites may jump to the ferric sites to make all the sites equal; for this exchange, the spin orientation on the four atoms must be the same (ferromagnetic case).

From this analysis, calculations lead to a surface termination that derives from the Fe_7O_8 slab (termination by two iron layers, ferromagnetic case). The reconstruction induces a switch in the upper layers (from rank 2 to rank 4). Therefore, the order of the layers from the surface toward the bulk is as follows: first, a single layer of iron atoms coordinated to the three atoms O_B of the layer beneath; the atoms O_A come next and the 'Td' iron layer as the fourth layer, close to the empty site of the dense layer. The main driving force for the permutation is the reduction of the local dipole perpendicular to the surface. The switch allows the positive charges of the ferrous and ferric ions to be distributed on both sides of the first oxygen

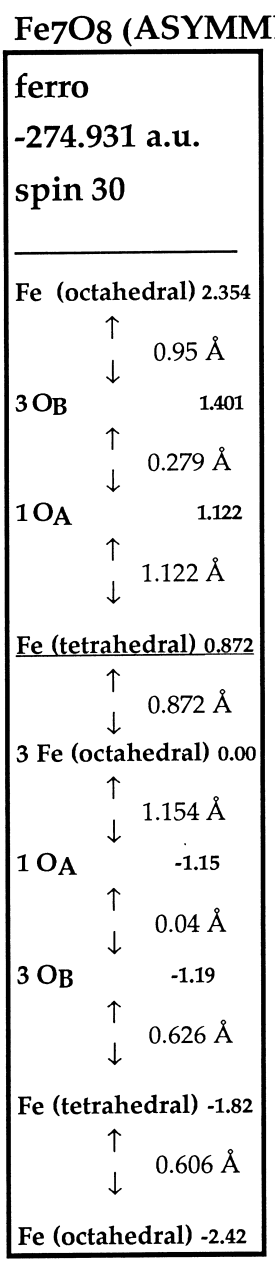

Fig. 11. Optimized calculated interlayer spacings for the Fe_7O_8 relaxed slab in the asymmetric model. The heights of the atoms of the upper part with positive values have been optimized; those of the lower part have been fixed to the experimental values. Layers that are switched (with a different ordering from that of the bulk) are underlined.

layer. This local reduction is not necessary in the symmetric model that has been constructed to cancel the global dipole moment. The reduction obtained by the permutation is local for the surface layers and thus more representative of the top layers of the surface standing on an unperturbed bulk.

If thermodynamically favored, the O switch requires passing a barrier when the iron and oxygen atoms are coplanar; this barrier may increase if the lattice parameter is reduced by the requirements of the epitaxial growth.

We first hoped that the switch could explain the LEED structure, since it leads to an apparent termination by a single iron monolayer. However, the interlayer spacings do not compare very well; in particular, the O_B atoms remain above the O_A atoms. Tensor LEED calculations do not match this description, and in Section 6, we propose a possible explanation and solution.

6. Hydrogenated surface

Since the Fe_5O_8 slab involves an excessive oxidation state, a reduction is necessary to lead to a stable slab. As hydrogen atoms are difficult to detect by LEED, reduction by hydrogen could provide a solution to the contradiction between LEED and total energy results. The protonation of the O_A atoms leads to a $Fe_5O_6(OH)_2$ slab with a reasonable mean oxidation number, 14/5. The HF calculation did converge well, indicating an improved physical model. The formal adsorption energy of H_2, 61.6 kcal/mol, and the binding energy for the O_A-H bonds, 71.7 kcal/mol, are large for the UHF results, indicating that the H atoms are strongly attached to the O_A atoms. The DOS corresponds to an insulator. The interlayer spacings are shown in Fig. 12. The O_A atoms move outside the O_B atoms at variance with the bulk structure and in agreement with LEED and PD studies. The interlayer spacing, Δ_2, is 0.10 Å vs. -0.04 Å in the bulk and 0.40 Å in Ref. [25]. Our parameters do not vary significantly for the variation of the lattice parameter (cases of epitaxial growth) or by taking into account the correlation (P91), and similar relaxations are obtained by hydrogenating the top face of the Fe_6O_8 slab (Fig. 13). Finally, the displacement of the O_A atoms is easily understood by the changes in coordination. At the surface, they become three-fold-coordinated and become closer to the basal plane of the tetrahedral site (the dense layer); this motion is more important than that for the O_B atoms that become dicoordinated, bridging two atoms from the dense layer. When a proton binds to the O_A atom, it pulls it in its direction since it is the strongest ligand and the apparent displacement is outward. We therefore interpret the LEED results as being consistent with the hydrogenation of the O_A atoms.

Surfaces are sensitive to the presence of hydrogen. The hydrogenation is possible when the oxidation state of the surface atoms allows a reduction. The $Fe_6O_7(OH)$ slab (three ferrous and three ferric ions) can be hydrogenated to lead to the $Fe_6O_4(OH)_4$ slab (six ferrous ions) that is terminated by hydroxyl groups. Then, the O_B atoms also move outward, and a switch occurs moving the iron surface layer inward, close to the dense layer (Fig. 13). This example, which does not correspond with the experimental result, shows that the surface geometry would be again modified by a complete hydrogenation and that, when the hydrogen atoms are not visualized, the relaxations can be an indirect signature of the presence or absence of invisible hydrogen atoms.

7. Conclusions

From the comparison of the calculated cohesive energies for different slabs, we conclude that the most stable termination for the clean surface consists of two outermost iron monolayers with a possible permutation between the second layer and the next deeper oxygen layer. The top layer is made of ferrous ions that originate from the octahedral interstitial sites of the fcc oxygen bulk lattice. Without permutation, this is in agreement with a visual interpretation of STM images [26,27], but in disagreement with more detailed LEED [25] and PD analyses [9]. It is consistent with the termination found in other spinel compounds such

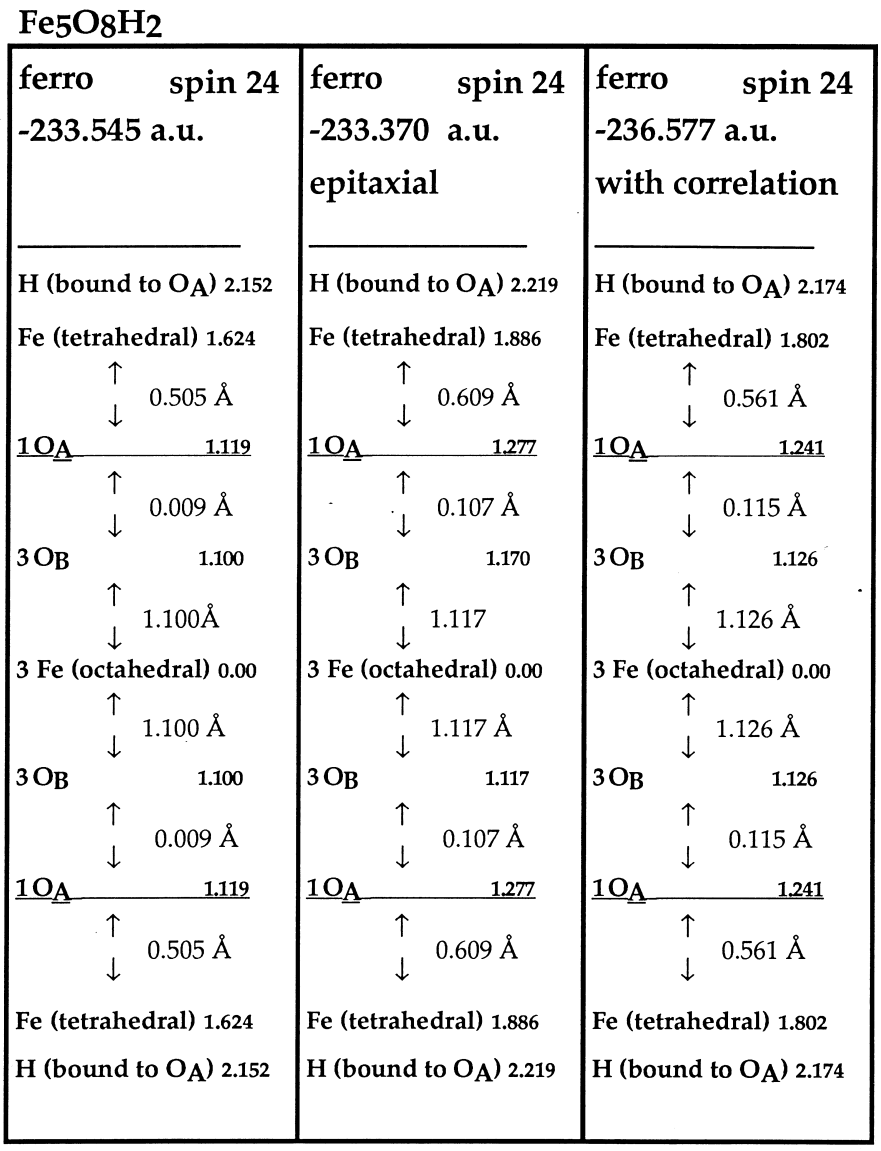

Fig. 12. Optimized calculated interlayer spacings for the $Fe_5O_6(OH)_2$ relaxed slab. The lattice parameter, 5.94 Å, has been reduced to 5.54 Å in the 'epitaxial' calculation. Optimized results with correlation are obtained using energies with P91 [29]. Layers that are switched (with a different ordering from that of the bulk) are underlined.

as $MgAl_2O_4$ whose faces are stable when they are terminated by Mg^{2+} monolayers [59]. The Fe_3O_4 (111) surface relaxes strongly. The stability of the termination depends on three main factors:

- The formal cleavage that generates the surfaces must break the smallest possible number of bonds.
- The surface atoms are cations in low oxidation

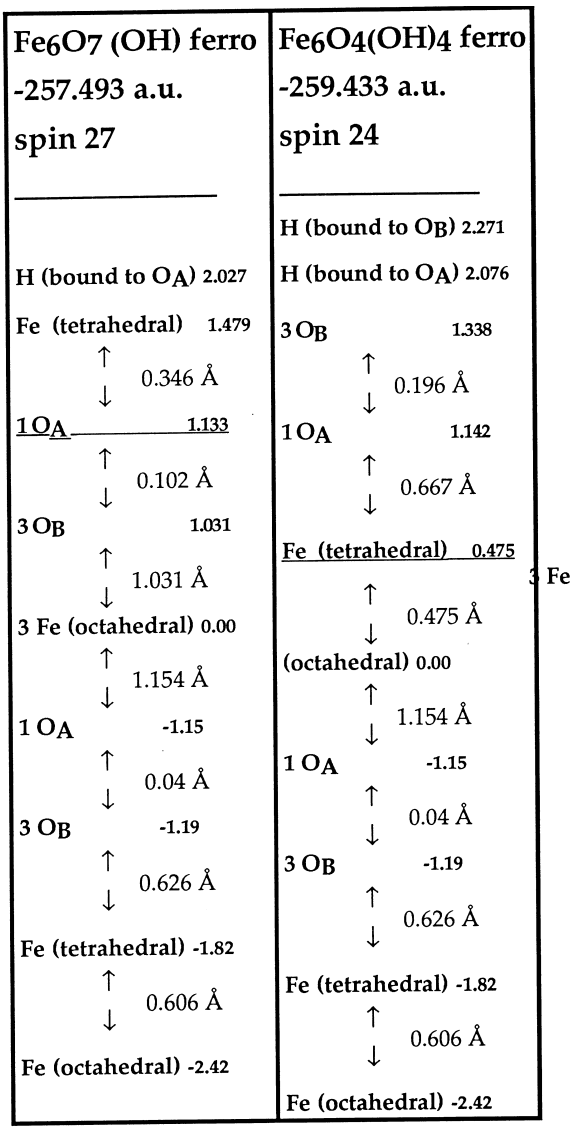

Fig. 13. Optimized calculated interlayer spacings for the $Fe_6O_7(OH)$ and $Fe_6O_4(OH)_4$ relaxed slabs. Calculations include correlation (P91). Layers that are switched (with a different ordering from that of the bulk) are underlined.

states. This, together with the relaxation, contributes to a reduction of the dipole moment perpendicular to the surface.

- Deviations from stoichiometry should be as small as possible. Since it is easy to reduce the ions from ferric to ferrous and difficult to oxidize the oxygen dianion, the surface must be oxygen-deficient.

Finally, we interpret the termination by two iron layers proposed from STM as being optimal for the clean surface, whereas the LEED and PD measurements are proposed to correspond to a partial hydrogenation with OH groups at the A sites.

Acknowledgements

M.A.V.H. and G.A.S. were supported in part by the Director, Office of Science, Office of Basic Energy Sciences, Materials Sciences Division of the US Department of Energy under contract No. DE-AC03-76SF00098. J.A. and C.M. acknowledge the IDRIS, CNRS National Supercomputing Center, for computing facilities.

References

[1] J.C. Mallinson, The Foundations of Magnetic Recording, 2nd edition, Academic Press, New York, 1993.
[2] R.K. Wild, in: D.R. Randall, W. Neagle (Eds.), Surface Science Analysis and Applications, Special Publication, Royal Society of Chemistry, London, 1990, p. 73.
[3] W. Geus, Appl. Catal. 25 (1986) 313.
[4] P.W. Tasker, J. Phys. C 12 (1979) 4977.
[5] R. Dovesi, V.R. Saunders, C. Roetti, Crystal 95, User Documentation, University of Torino and SERC Daresbury Laboratory, 1996.
[6] H.C. Galloway, J.J. Benitez, M. Salmeron, J. Vac. Sci. Technol. A 12 (1994) 2302.
[7] G.H. Vurens, V. Maurice, M. Salmeron, G.A. Somorjai, Surf. Sci. 268 (1992) 170.
[8] W. Weiss, G.A. Somorjai, J. Vac. Sci. Technol. A 11 (1993) 2138.
[9] Y.J. Kim, C. Westphal, R.X. Ynzunza, Z. Wang, H.C. Galloway, M. Salmeron, M.A. Van Hove, C.S. Fadley, Surf. Sci. 416 (1998) 68–111.
[10] Y.J. Kim, C. Westphal, R.X. Ynzunza, H.C. Galloway, M. Salmeron, M.A. Van Hove, C.S. Fadley, Phys. Rev. B 55 (1997) 1344.
[11] H.C. Galloway, P. Sautet, M. Salmeron, Phys. Rev. B 54 (1996) 11145.
[12] C. Rehbein, N.M. Harrison, A. Wander, Phys. Rev. B 54 (1996) 14066.
[13] M. Gautier-Soyer, M. Pollak, L. Henriot, M.J. Guittet, Surf. Sci. 352–354 (1996) 112.
[14] W. Weiss, Surf. Sci. 377–379 (1997) 943.

[15] T. Schedel-Niedrig, W. Weiss, R. Schlögl, Phys. Rev. B 52 (1995) 17449.
[16] S.K. Shaikhutdinov, W. Weiss, Surf. Sci. 432 (1999), L627.
[17] R.J. Lad, V.E. Henrich, Surf. Sci. 193 (1988) 81.
[18] W. Weiss, A. Barbieri, M.A. Van Hove, G.A. Somorjai, Phys. Rev. Lett. 71 (1993) 1848.
[19] E. Wasserman, J.R. Rustad, A.R. Felmy, B.P. Hay, J.W. Halley, Surf. Sci. 385 (1997) 217.
[20] L. Armelao, M. Bettinelli, M. Casarin, G. Graznozzi, E. Tondello, A. Vittadini, J. Phys. Condens. Matter 7 (1995) L299.
[21] X.G. Wang, W. Weiss, S.K. Shaikhutdinov, M. Ritter, M. Petersen, F. Wagner, R. Schlögl, M. Scheffler, Phys. Rev. Lett. 81 (1998) 1038.
[22] M. Catti, G. Valerio, R. Dovesi, Phys. Rev. B 51 (1995) 7441.
[23] M. Catti, G. Sandrone, G. Valerio, R. Dovesi, J. Phys. Chem. Solids 11 (1996) 1735.
[24] M. Causa, C. Pisani, C. Roetti, Surf. Sci. 215 (1989) 259.
[25] A. Barbieri, W. Weiss, M.A. Van Hove, G.A. Somorjai, Surf. Sci. 302 (1994) 259.
[26] N.G. Condon, P.W. Murray, F.M. Leibsle, G. Thornton, A.R. Lennie, D.J. Vaughan, Surf. Sci. 310 (1994) L609.
[27] A.R. Lennie, N.G. Condon, F.M. Leibsle, P.W. Murray, G. Thornton, D.J. Vaughan, Phys. Rev. B 53 (1996) 10224.
[28] W. Weiss, M. Ritter, Phys. Rev. B 59 (1999) 5201.
[29] P. Perdew, Unified Theory of Exchange and Correlation Beyond the Local Density Approximation, Nova Science, New York, 1991.
[30] M. Causa, R. Colle, A. Fortunelli, R. Dovesi, C. Pisani, Phys. Rev. 36 (1987) 891.
[31] M. Causa, R. Colle, A. Fortunelli, R. Dovesi, C. Pisani, Phys. Scr. 38 (1988) 194.
[32] N.M. Harrison, V.R. Saunders, E. Apra, M. Causa, R.J. Dovesi, J. Phys.: Cond. Matt. Lett. 4 (1992) 261.
[33] P. Durand, J.C. Barthelat, Theor. Chim. Acta 38 (1975) 283.
[34] R.W.G. Wyckoff, in: Crystal Structures, 2nd edition. Vol. 2 (1982) 5.
[35] Y. Bouteiller, C. Mijoule, M. Nizam, J.C. Barthelat, J.P. Daudey, M. Pelissier, B. Silvi, Mol. Phys. 65 (1988) 295.
[36] A. Dargelos, private communication.
[37] C.E. Moore, in: Atomic Energy Levels, Natl. Bur. Stand., Washington, DC, Vol. II (1952).
[38] C.E. Moore, in: Atomic Energy Levels, Natl. Bur. Stand., Washington, DC Vol. I (1949).
[39] L. Salasco, R. Dovesi, R. Orlando, M. Causa, V.R. Saunders, Mol. Phys. 72 (1991) 267.
[40] M. Causa, R. Dovesi, C. Roetti, C. Kotomin, V.R. Saunders, Chem. Phys. Lett. 140 (1980) 120.
[41] C.N.R. Rao, J. Gopalakrishnan, New Directions in Solid State Chemistry, Cambridge University Press, Cambridge, 1986.
[42] P.A. Cox, Transition Metal Oxides: An Introduction to their Electronic Structure and Properties, Clarendon Press, Oxford, 1992.
[43] F.C. Voogt, T. Hibma, G.L. Zhang, M. Hoefman, L. Niesen, Surf. Sci. 331–333 (1995) 1508.
[44] R.C. Weast (Ed.), CRC Handbook of Chemistry and Physics, 58th edition, CRC Press, Cleveland, 1978, p. D71.
[45] C. Noguera, Physique et Chimie des surfaces d'oxydes, Collection Aléa Saclay, Eyrolles and CEA, Paris, 1995.
[46] N. Floquet, L.C. Dufour, Surf. Sci. 126 (1983) 543.
[47] V.E. Henrich, Surf. Sci. 57 (1976) 385.
[48] H. Onishi, C. Egawa, T. Aruga, Y. Iwasawa, Surf. Sci. 191 (1987) 479.
[49] M.A. Van Hove, P.M. Echenique, Surf. Sci. 82 (1979) L298.
[50] M. Tsukada, T. Hoshino, J. Phys. Soc. Jpn. 50 (1982) 3032.
[51] A. Pojani, F. Finocchi, J. Goniakowski, C. Noguera, Surf. Sci. 387 (1997) 354.
[52] S. Eriksen, R.G. Egdell, Surf. Sci. 180 (1987) 263.
[53] S. Bourgeois, F. Jomard, M. Perdereau, Surf. Sci. 279 (1992) 349.
[54] P.W. Murray, F.M. Leibsle, C.A. Muryn, H.J. Fischer, C.F.J. Flipse, G. Thornton, Surf. Sci. 321 (1994) 217.
[55] P.W. Murray, F.M. Leibsle, C.A. Muryn, H.J. Fischer, C.F.J. Flipse, G. Thornton, Phys. Rev. Lett. 72 (1994) 689.
[56] D.F. Cox, T.B. Fryberger, S. Semacik, Surf. Sci. 224 (1989) 121.
[57] H. Tanaka, T. Matsumoto, T. Kawai, S. Kawai, Surf. Sci. 318 (1994) 29.
[58] G. Renaud, B. Villette, I. Vilfran, A. Bourret, Phys. Rev. Lett. 73 (1994) 1825.
[59] M.J. Davies, S.C. Parker, G.W. Watson, J. Mater. Chem. 4 (1994) 813.
[60] K.P. Huber, G. Herzberg, Molecular Spectra and Molecular Structure IV. Constants of Diatomic Molecules, Van Nostrand, Princeton, NJ, 1979.